Photophysics of H- and J-Aggregates of Indole-Based Squaraines in Solid State

ARTICLE *in* THE JOURNAL OF PHYSICAL CHEMISTRY C · MAY 2012

Impact Factor: 4.77 · DOI: 10.1021/jp210281z

7 AUTHORS, INCLUDING:

Gustavo de Miguel Rojas
University of Cordoba (Spain)
34 PUBLICATIONS **570** CITATIONS
SEE PROFILE

Marcin Ziolek
Adam Mickiewicz University
53 PUBLICATIONS **819** CITATIONS
SEE PROFILE

Shyam S Pandey
Graduate School of Life Science and Systems …
143 PUBLICATIONS **1,566** CITATIONS
SEE PROFILE

Shuzi Hayase
Kyushu Institute of Technology
203 PUBLICATIONS **2,384** CITATIONS
SEE PROFILE

THE JOURNAL OF PHYSICAL CHEMISTRY C

Article

pubs.acs.org/JPCC

Photophysics of H- and J-Aggregates of Indole-Based Squaraines in Solid State

G. de Miguel,[†] M. Ziółek,[†,§] M. Zitnan,[†] J. A. Organero,[†] S. S. Pandey,[‡] S. Hayase,[‡] and A. Douhal*[,†]

[†]Departamento de Química Física, Sección de Químicas, Facultad de Ciencias del Medio Ambiente, Universidad de Castilla-La Mancha, Av. Carlos III S/N, 45071 Spain

[‡]Kyushu Institute of Technology, 2-4 Hibikino, Wakamatsu, Kitakyushu, Japan

Supporting Information

ABSTRACT: The photodynamics of six types of indole-based squaraines (SQs) molecules deposited onto quartz substrates by using the spin-coating method have been studied by means of steady-state and time-resolved techniques. Enhanced scattering signal at the resonance wavelengths together with the broadening and shift of the absorption bands to the red side with respect to those in solution prove the formation of H- and J-aggregates in the thin film samples. Excited state deactivation dynamics were studied by the femtosecond (fs) transient absorption spectroscopy and nanosecond (ns) flash photolysis. Faster kinetics were obtained for the solid state samples as compared to those in solution. Singular value decomposition (SVD) analysis of the fs transient signal proves the presence of monomers and aggregates, enabling the separation of the kinetics for each one. For the SQ monomers, the dynamics of the singlet excited state does not depend on the pump fluence, and we thus propose that the quenching of the excited monomers is due to an energy transfer process to the aggregates. For the SQ aggregates, nonexponential fit of the experimental time profiles along with the power dependence of the transient absorption signal indicates a singlet−singlet annihilation process ($\gamma' \approx 3 \times 10^{-15}$ cm^3 s$^{-1/2}$). The combination of the long-range Förster-type mechanism and quantum delocalization is found to be the physical process that accounts for the singlet−singlet annihilation. In the flash photolysis experiments, we observed transient signals with a maximum intensity at 710 nm and lifetimes of 30 and 35 ns for SQ 41 and SQ 26, respectively. We have attributed these signals to the *cis* photoisomers of the aggregates deactivating to the *trans* photoisomers through the back photoisomerization reaction. These results provide information for a better understanding of the photodynamics of squaraines.

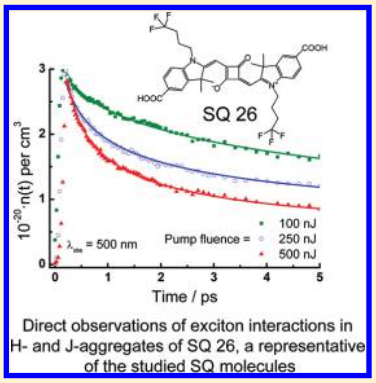

Direct observations of exciton interactions in H- and J-aggregates of SQ 26, a representative of the studied SQ molecules

1. INTRODUCTION

Molecular aggregates represent an intermediate situation between isolated molecules and pure crystal.[1] As such, they can be found widespread in nature, functioning in most of the photobiological processes, including photosynthesis.[2,3] For example, molecular aggregates take part in the majority of the energy or charge transfer processes that occur in living organisms.[4] However, aggregates continue to be an area of significant current interest driven mainly by promising commercial applications including light-emitting diodes and solar cells.[5−7] Self-assembly of molecules and their integration into functional devices is a challenging field of modern science and technology.[8] J-aggregates are nice examples of the self-assembled structures, where self-assembly crucially changes their spectral and other functional properties.[1,9−12] The utmost importance of these systems resides in the extraordinary optical properties of these molecular aggregates, which are to a large extent governed by exciton delocalization, transport, and relaxation phenomena.[1,13−17] It is necessary to understand the optical properties of molecular dye aggregates to optimize their performance for technological application.

Squaraines (SQs) represent a family of chromophores with a high tendency to form aggregates even in solution.[18] They belong to the class of polymethyne dyes with resonance-stabilized zwitterionic structure, with a donor−acceptor−donor (D−A−D) charge transfer interaction.[19] The HOMO−LUMO gap in SQ molecules depends on two factors: the extension of the π-electron delocalization and the electron donating properties of the side groups.[20] Thus, the nature of the electron donating groups defines the tunable optical properties of the SQs, i.e., *N*,*N*-dialkylanilines,[21] benzothiazoles,[22] phenols,[23] azulenes,[24] pyrroles,[25] or indoles.[26]

The extraordinary optical properties of the SQs have generated considerable interest to use them for multiple applications.[19b] SQs can be used as chemosensors,[19a] in which an ionophore unit attached to the SQ produces a modification of the absorption and emission properties under the influence of external stimuli, like different ions, pH, temperature, etc.[27] In this respect, exciton interaction in SQ aggregates may function as a potential signaling pathway of a specific ion-binding event. This is a topic of considerable interest because of their importance in specific detection of analytes in different fields

Received: October 26, 2011
Revised: April 12, 2012
Published: April 16, 2012

   dx.doi.org/10.1021/jp210281z | *J. Phys. Chem. C* 2012, 116, 9379−9389

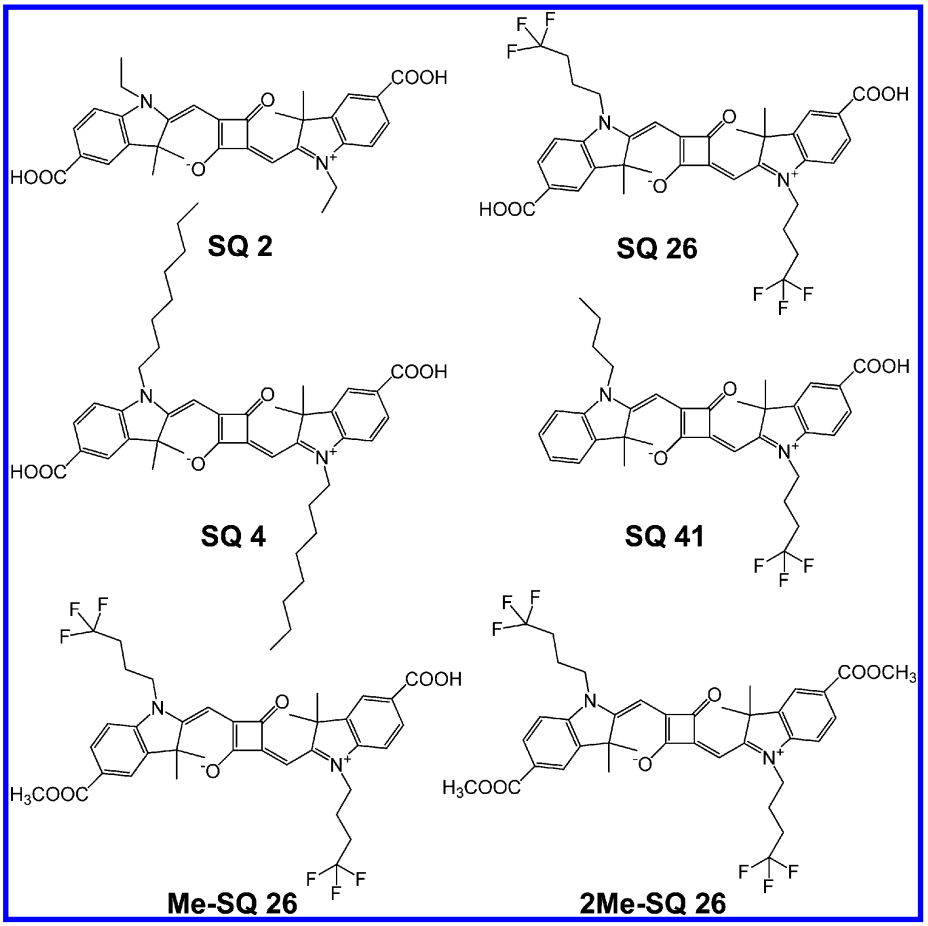

Figure 1. Molecular structures of the six studied SQ compounds.

such as chemistry, biology, medicine, and environmental science. SQs have also been employed as second generation photosensitizers for photodynamic therapy.[19b] Prevention of aggregation is a desirable property to enhance cell permeability and perform their photodynamic effect.[28] Nonsymmetric SQs can also behave as second harmonic generation (SHG) derivatives due to deviation from a symmetric electronic distribution.[19b,29] This interest is related to the exploitation of this property in low-cost electro-optic devices such as high-speed photonic switching and electro-optic modulators.[30] Aggregation of SQs can play a major role in changing the molecular quadratic hyperpolarizability since these devices are fabricated in solid state. Finally, its ability to extend the absorption spectrum to the NIR wavelength range by judicious selection of suitable donor moieties with extended π-conjugation together with its photostability makes them ideal candidates to be used as photosensitizers in dye-sensitized solar cells (DSSCs).[31] However, their lower efficiency of sunlight conversion due to H-aggregate formation needs more logical dye design, synthesis, and study.[32] A comprehensive understating of the photophysics of SQ dyes, in particular the rapid quenching of the excited states in the solid state, and the relationship of these processes to the aggregation behavior will be highly beneficial for the design and development of SQ-based solid-state devices for multiple applications.

In this work, we report on the photophysics of indole-based SQs in the solid state by a combination of steady-state and time-resolved techniques, with the aim of a better understanding of their excited-state properties. These SQs have attached one or two carboxylic/methyl ester groups in the indole moiety (Figure 1). Substitution at the N-position of the indole groups, ethyl, butyl, octyl, or trifluorobutyl alkyl chains makes also a difference among the six SQs. Solid samples were prepared as thin films, deposited on a quartz plate by the spin-coating method. Our results show the presence of two transient species in the excited state, monomer and H- and J-aggregates, which deactivate through a fast energy transfer process and a singlet−singlet annihilation mechanism, respectively. We believe that the photophysical information that is presented in this work will be valuable to gain an insight into the relationship between structural properties and potential applications of SQs.

2. EXPERIMENTAL PART

The six studied SQ molecules, whose general structures are shown in Figure 1, were synthesized as it is described elsewhere.[26] Solid samples were prepared by the spin-coating method, obtaining a homogeneous thin film of 60−70 nm in thickness. No major photodegradation was detected within the days we measure the samples. However, solid samples were measured as fast as possible after their preparation to avoid the influence of external parameters in the photodynamics. The preparation steps are as follows: (a) cleaning of quartz plates in isopropanol at ultrasonic bath for 10 min; (b) drying under the stream of nitrogen; (c) preparation of SQ dye solution in 1:1 mixture of chloroform and pyridine having concentration of 10 mg/mL; (d) spin-coating on cleaned quartz substrate by spinning at 1500 rpm for 30 s followed by 3000 rpm for 60 s;

dx.doi.org/10.1021/jp210281z | J. Phys. Chem. C 2012, 116, 9379−9389

(e) drying the sample on hot plate at 120 °C for 10−15 min; (f) thickness measurement using DEKTAK surface profiler indicates a thickness from 60 to 70 nm. Acetonitrile (ACN), spectroscopic grade (>99.5%), purchased from Sigma-Aldrich was used as received. UV−vis steady-state absorption spectra were measured with a JASCO V-670. Resonance light scattering measurements were conducted on a FluoroMax-4 (Jobin-Yvone) in the synchronous scanning mode in which the emission and the excitation monochromators are present to identical wavelengths.

Femtosecond (fs) UV−vis transient absorption spectra were measured using a two-channel detection system described previously.[33] It consists of a Ti:sapphire oscillator (TISSA 50, CDP Systems) pumped by a 5 W diode laser (Verdi 5, Coherent). The seed pulse (30 fs, 450 mW at 86 MHz) centered at 800 nm wavelength is directed to an amplifier (Legend Ultra-Short-Pulse, Coherent). The amplified fundamental (50 fs, 1 W at 1 kHz) is directed through an optical parametric amplifier for wavelength conversion (CDP Systems) to a femtosecond-transient absorption spectrometer (CDP Systems), where it is split into two beams. The first one is frequency-doubled to give 630−670 nm for exciting the sample. The remaining fundamental beam goes through a delay line and is focused on a rotating 3 mm thick CaF_2 plate to generate the white light continuum. The produced white light is split into two parts to form probe and reference beams, which are directed to the sample adsorbed on a quartz plate, where the probe and the pump beams are overlapped. The cell is placed on translation stages (MTS series, Thorlabs). This moves the sample in the $x-y$ plane perpendicular to the pump beam to prevent it from photodegradation. The polarization of the pump is set to magic angle with respect to the probe. The transmitted light is directed to a spectrograph and collected by a pair of photodiode arrays.

The UV−visible ns−s flash photolysis setup consists of LKS.60 laser flash photolysis spectrometer (Applied Photophysics), Vibrant (HE) 355 II laser (Opotek) as a pump pulse source (5 ns time duration), and a 150 W xenon arc lamp as a probe. The light from an optical parametric oscillator, OPO (355 nm pumped by Q-switched Nd:YAG laser, Brilliant, Quantel), in the wavelengths range between 590 and 680 nm was used for sample excitation. The probing light source was a 150 W xenon arc lamp. The light of the probe transmitted through the sample was dispersed by a monochromator and detected by a photomultiplier coupled to a digital oscilloscope (Agilent Infiniium DS08064A, 600 MHz, 4 GSa/s). The pump pulse energy (9 mJ/pulse) was attenuated by a pair of half-waveplate and a polarizer. The signal was recorded in the spectral range of 550−750 at 10 nm interval, and the time-resolved absorption spectra were constructed from the kinetic traces fitted by a global analysis program (PC ProK, Applied Photophysics). The quality of the fits was checked by examining the residual distribution and the χ^2 value. All the experiments were done at 293 K.

3. RESULTS AND DISCUSSION

3.1. Steady-State UV−vis Absorption Spectroscopy. Figure 2 shows the UV−vis absorption spectra of the six SQs in acetonitrile (ACN) solutions. We found narrow absorption bands with the absorption maxima around 645 nm for the studied SQs. A high-energy vibrational transition was also observed around 600 nm, but with a lower intensity. Interestingly, the absorption spectra present similar bandwidths

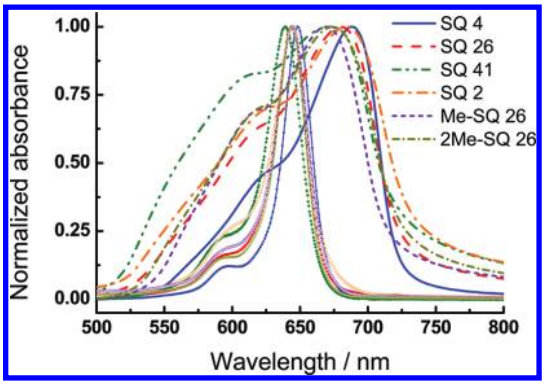

Figure 2. Normalized UV−vis steady-state absorption spectra of SQ 4 (solid line), SQ 26 (long-dashed line), SQ 2 (long-dashed dotted line), SQ 41 (dashed double-dotted line), Me-SQ 26 (short-dashed line), and 2Me-SQ 26 (short-dashed dotted line) deposited as thin films on a quartz plate. For comparison, the spectra in ACN are shown.

and not very different wavelengths at the intensity maxima for the six SQs. This is explained on the basis of the poor influence of the substituents on the donor−acceptor−donor interaction in these indole-based SQs. In addition to that, a previous work[34] has excluded the presence of aggregates in solution through concentration-independent absorption spectra and fluorescence anisotropy experiments.

An opposite trend was found when studying the solid films, prepared by the spin-coating method on quartz substrates. First, the absorption spectra exhibit a much broader band when compared to those in solution (Figure 2). Second, the absorption maxima are shifted to the red region. The maxima of intensity are around 678 nm for the studied SQs, and pronounced shoulders appear at 625 nm. Third, the relative ratio between the intensity of the maximum absorption and the shoulder is higher than that in solution. To further prove the formation of aggregates, resonance light scattering (RLS) experiments were carried out. Figure S1 illustrates the RLS spectra vs absorption ones for three SQs. The scattering signal is enhanced in the vicinity of the absorption bands, showing a similar shape to that of the absorption spectra, but the maximum of the peak is shifted to the red. Based on the above observations, H- and J-aggregates of the studied SQs form in thin films. The close proximity of the molecules makes the exciton interaction possible, producing the splitting of the molecular orbitals.[1,18] A deconvolution of the absorption spectra require three Gaussian functions to accurately fit the experimental curve (Figure S2). Mismatch between experimental curve and the fit at wavelengths longer than 725 nm is due to the presence of several minor populations of J-aggregates, which cannot be fitted by using only one Gaussian function. Comparison among the six SQs shows that the Gaussian curve associated with the H-aggregate is more prominent in SQ 41 and less intense in SQ 4. Considering that H- and J-aggregates consist of a face-to-face and face-to-tail interaction between molecules, respectively, we may assert that H-aggregate formation is less favored in SQ 4 since the long alkyl chains introduce a stronger steric hindrance. However, shorter alkyl chains and, most importantly, the absence of one carboxylic group (electrostatic repulsions), in SQ 41, promote H-aggregate formation. Additionally, in SQ 2 having the shortest alkyl chains, H-aggregate formation is less favored than in SQ 41, and it is similar to that in SQ 26. Finally, methylation

dx.doi.org/10.1021/jp210281z | J. Phys. Chem. C 2012, 116, 9379−9389

of the carboxylic groups in SQ 26 does not alter the percentage of H-aggregate in Me-SQ 26 and 2Me-SQ 26.

In summary, the studied SQs molecules are present in solution as monomers with narrow absorption bands. In opposition to that, enhanced scattering signal at the resonance wavelengths together with the broadening and shift of the absorption bands to the red side with respect to those in solution prove the formation of H- and J-aggregates. Different ratios between the two bands in the thin films are due to the distinct ability to form H-aggregates for each SQs.

3.2. Femtosecond Transient Absorption Measurement. With the aim of understanding the relaxation pathways that takes place upon electronic excitation of the SQs films, we have carried out femtosecond (fs) UV−vis transient absorption pump−probe experiments. Figures 3 and Figure S3 show the

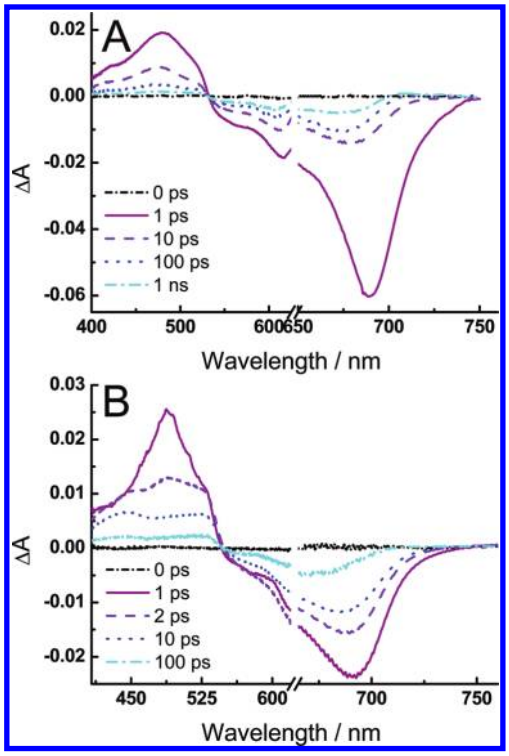

Figure 3. Femtosecond transient absorption spectra of SQ 41 (A) and SQ 26 (B) deposited as a thin film on a quartz plate at five delay times.

transient absorption spectra at different pump−probe delays and exciting at 640 nm. Interestingly, we notice that the spectra —shape and wavelength— up to 1 ps resemble those in solution,[34] but in contrast to the behavior in solution, the shape of the transient features changes when the delay time becomes longer. Thus, the initial transient peaks around 490−540 nm moves to 480 nm in SQ 41 and evolves in a broad band for the other SQs. The different spectral shifts come from a different evolution of the initial transient species formed upon photoexcitation (vide infra). It is worth noting the broad bleach of the transient signals between 550 and 725 nm for the studied SQs, which matches very well the corresponding steady-state absorption spectrum. These negative signals suggest a ground state depopulation of the H- and J-aggregates in thin films. However, a contribution of the stimulated emission to the negative signal is not completely ruled out since the Stokes shift (300 cm^{-1}) is very small in these SQs.[34] At longer delays (≈1 ns), an extremely weak positive transient signal at 710 nm is observed (Figure S4), which stays stable up to 1.6 ns. We will discuss the origin of this transient signal in the Flash Photolysis section.

In order to investigate the origin of the changes in the fs−ps transient features, we carried out a global analysis of the data. Thus, three or four exponential functions, depending on the sample, were used to accurately fit the data. Figure 4 and Figure

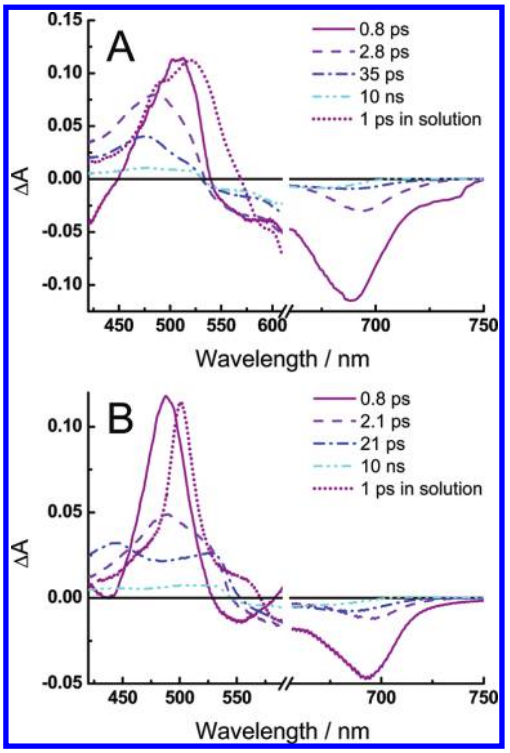

Figure 4. Associated transient absorption spectra for SQ 41 (A) and SQ 26 (B) deposited as thin films on a quartz plate obtained from a multiexponential global analysis of the data. Δ*A* is the change in the photoinduced absorbance of the sample. The time constants for each spectrum are shown in the inset. 1 ps transient absorption spectra in ACN solution are shown as a comparison (dotted lines). The spectrum at 10 ns time constant is obtained by fixing this value in the fit.

S5 give the obtained associated transient spectra of each component. Transient spectra in ACN solution are also shown for comparison. We obtained narrow bands for the associated transient spectra of the fastest components (<1 ps), with the exception of SQ 41 which gives a slightly broader spectrum in the blue side. On the other hand, a broad band for all the SQs films was derived for the other long-living components (>1 ps) at the 420−550 nm region, which suggests that it is originating from the same transient species. Therefore, long-living species deactivate in a complex way which reflects a heterogeneous population of the samples. At least two species are present in the excited state with different transient spectra.

We ascribed the fast component in the solid state to the signal of the first singlet excited state of the SQ monomers since the associated transient spectra are quite similar to the transient absorption spectra in solution (see Figure 4 and Figure S5). The only mismatch is the shift to the blue (10−20 nm) of the maximum of the signal in the solid samples. This is due to a different molecular environment of the SQs in the thin films when compared to that in solution. The observed shift in the transient maxima when probing these SQs in different

dx.doi.org/10.1021/jp210281z | J. Phys. Chem. C 2012, 116, 9379−9389

solvents supports our explanation.[34] In addition to that, the broader bleaching signal in the solid sample may affect the position of the transient maxima. The long-living component (>1 ps) is attributed to the singlet excited state of the H- and J-aggregates. The broad associated spectra for the aggregates support this assignment since the heterogeneity of the aggregates in the solid sample will lead to a broadening of the spectrum.

We have compared the time profiles at 520 nm of the solid samples with regard to those obtained for the same SQs dissolved in acetonitrile solutions. Figure S6 illustrates the results for SQ 41 (A) and SQ 26 (B). Clearly, the photodynamics are faster for the solid samples. When fitting the intensity decays of these samples, we used a multiexponential function, reflecting the complexity of the deactivation mechanism. To separately investigate the photodynamics of the aggregates, we excited at 600 nm (H-aggregates) and 670 nm (J-aggregates). We found no remarkable differences in the transient behaviors (similar shape of the transient spectra and kinetics at the different wavelengths), which suggests that the deactivation mechanism is independent of the reached excited state, whether monomers, H- or J-aggregate, and reflecting a very fast conversion between them at S_1.

In summary, multiexponential global analysis of the data revealed the presence of two main transient components. The associated transient spectra for the fastest component are similar to those spectra in solution; therefore, the corresponding signal is ascribed to the deactivation of the first singlet excited state of the monomer species. On the other hand, the associated transient spectra for the long-living components (>1 ps) are quite similar to each other, being attributed to the first singlet excited state of the H- and J-aggregates. The photodynamics are considerably faster in thin films when compared to that in solution.

3.3. Fluence Dependence of the Femtosecond Experiments. The faster kinetics in the thin films as compared to that in solution suggests rapid recombination processes that take place in the solid samples. This is an indication of the presence of self-quenching events that usually occur in solid-state relaxation. Annihilation is commonly responsible for these deactivation channels, and it exhibits a strong dependence of the signal on the fluence of the pump.[35] Therefore, to explore this possibility, we have performed fs transient absorption measurements at three different laser fluences, 100, 250, and 500 nJ/pulse, for SQ 41 and SQ 26 solid-state samples.

The results revealed that for both SQs the decays are faster for higher pump fluence (Figure 5). As we previously noted, we have a participation of at least two species in the total transient absorption decay: H- and J-aggregates with broad transient absorption band and longer lifetimes, along with the monomer species with a shorter decay and a narrower absorption band. Thus, quantitative analysis of their decay dependence on the excitation fluence requires separation of the related kinetics. Unfortunately, we could not find an observation wavelength that can be considered as exclusive to one of the species, and at which a fit might be performed with a good signal-to-noise ratio.

Therefore, in order to analyze the pump fluence dependence of the signal of each species, we applied singular value decomposition (SVD) analysis to the transient absorption data. For simplicity, we considered the H- and J-aggregates having the same fluence dependence of their signals and therefore

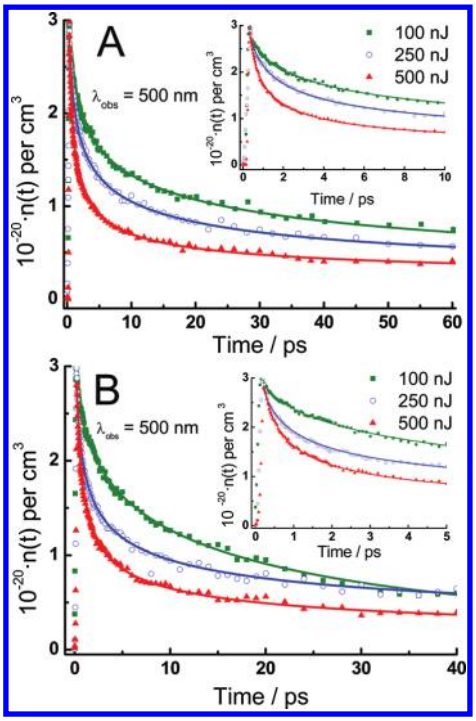

Figure 5. Time profiles, after singular value analysis (SVD), of SQ 41 (A) and SQ 26 (B) transient absorption signal at 500 nm using different pump fluences (excitation at 640 nm), 100, 250, and 500 nJ/pulse. The solid lines correspond to the best fits of the experimental data using eq 3. The time profiles at 100 and 250 nJ/pulse were normalized to the intensity of that at 500 nJ/pulse. $n(t)$ is the density of the singlet excited states of the aggregates.

similar individual photobehaviors. The SVD analysis gives singular values of the two-dimensional matrix constructed from time-dependent and wavelength-dependent signals, and the so-called spectral and time vectors associated with each singular value.[36−38] According to the theory for matrixes,[36] the number of singular values obtained in such analysis, which is greater than the noise, is equal to the number of species participating in the observed dynamics over the whole investigated spectral range. Moreover, the spectral and time vectors associated with these singular values represent linear combinations of the individual spectra and kinetics of each species.

The first six singular values obtained for SQ 26 and SQ 41 for different pump fluences measured in the 405−625 nm spectral range are summarized in Table 1. As we can see, in most cases only the first two singular values are considerably higher than the rest, which do not differ too much between each other. The spectral vectors associated with the first and second singular values are shown in Figures S9 and S10, respectively. The spectral and kinetics vectors of the singular values other than the first two exhibit either unstructured shape or noisy distribution, which indicates that they cannot represent a real behavior. Thus, the SVD analysis confirms the participation of two main species in the evolution of the transient absorption signals of the solid samples.

The spectral vector of the first dominant singular value (Figure S9) is the same at different fluences, and it is very similar to the transient absorption spectra measured at long times (>1 ps). Therefore, we assign it to the aggregate species, and the kinetic vector associated with it can be considered as showing exclusively the population change of the aggregates. In turn, the spectral and kinetics vector of the second singular

dx.doi.org/10.1021/jp210281z | J. Phys. Chem. C 2012, 116, 9379−9389

Table 1. Six First Singular Values Obtained from the Singular Value Analysis (SVD) of the Transient Absorption Signal of SQ 41 and SQ 26 Deposited as Thin Films on a Quartz Plate at the Different Fluences of the Pump, 100, 250, and 500 nJ/pulse (Excitation Wavelength 640 nm)

	SQ 26			SQ 41		
	pump fluence (nJ/pulse)			pump fluence (nJ/pulse)		
singular value number	100	250	500	100	250	500
1	1.001 82	1.900 92	3.654 58	1.084 84	2.619 45	5.456 84
2	0.162 4	0.273 35	0.494 87	0.136 74	0.278 7	0.764 14
3	0.099 95	0.124 95	0.177 36	0.079 36	0.161 29	0.236 31
4	0.073 01	0.106 53	0.099 96	0.058 09	0.140 55	0.176 46
5	0.064 33	0.099 93	0.083 09	0.047 9	0.107 29	0.132 18
6	0.049 84	0.077 79	0.072 68	0.043 37	0.095 12	0.115 22

value can be assigned to the monomer species (Figures S10 and S11). It has to be pointed out that such successful spectral and temporal separation of the two species directly into spectral and kinetic vectors of SVD analysis was possible only because (i) we have two main species and (ii) at long times only one of them is present (aggregates). In general, and as stated before, the spectral and kinetic vectors do not have so straightforward interpretation since they are linear combinations of individual spectra and kinetics of the species, and an additional analysis is necessary to elucidate the latter.

On one hand, the monomer species of both SQ 26 and SQ 41 decay in a very fast way (~100 fs), and there is no clear dependence of their kinetics on the excitation fluence (Figure S11). This indicates that the quenching of the monomers is not due to the annihilation mechanism. The small negative values that are reached by the kinetic vector associated with them are probably due to not perfect separation of the species by SVD method and some influence of the noise. Moreover, the transient spectra of the monomers (Figure S10) do not show any negative feature in the spectral range corresponding to the stationary absorption band, which indicates that their decay is not connected with the recovery of the signal. Therefore, we propose that the quenching of the excited monomers is due to an energy transfer to the J-aggregates (in the ground state), since all the possible energy-transfer mechanisms (Förster, Dexter, or the trivial mechanism involving emission and reabsorption) imply a spectral overlap between the monomer emission and the absorption of the acceptor, which is only plausible with the J-aggregate and not with the H-aggregate (Scheme 1).

On the other hand, on the basis of previous findings, we propose a singlet−singlet exciton annihilation[35] process to be responsible for the deactivation of the excited aggregates, since no triplet features were detected by the fs−ns transient absorption experiments (triplet−triplet annihilation). Annihilation may occur between the same or different types of aggregates. Thus, the energy of one singlet excited state of the aggregates is transferred to another one, which is in close proximity, giving rise to one ground state species (S_0) and one highly excited state (S_n) (eq 1). Subsequently, the S_n ($n > 1$) state decays to the S_1 state which might again undergo the annihilation process. This mechanism permits to release energy from the S_1 state without radiative emission.

$$S_1 + S_2 \rightarrow S_0 + S_n \quad (1)$$

Figure 5 shows the time profiles of the transient absorption signal at 500 nm, close to the maximum of transient absorption band and under excitation at 640 nm and at different fluences of the pumping laser. In this figure, the contribution of the

Scheme 1. Energy Level Diagram (Not in Scale) for (A) Monomers and J-Aggregates and (B) H-Aggregates of SQ 41, Accounting for the Energy Transfer, Singlet−Singlet Annihilation, and Photoisomerization Reactions[a]

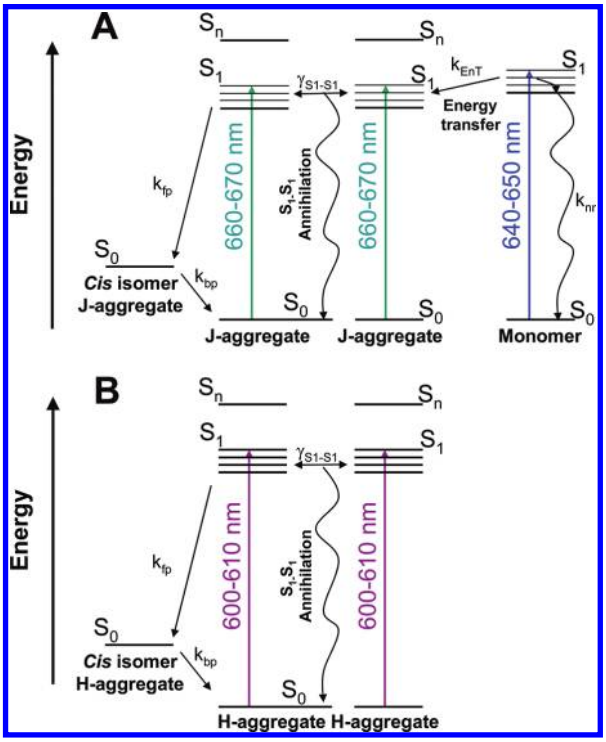

[a] $k_{nr} = 3.4 \times 10^9\ s^{-1}$ is the deactivation rate constant of monomers in the absence of any interaction between excitons. $k_{EnT} = 10^{13}\ s^{-1}$ is the rate constant for the energy transfer process. $\gamma'_{S-S} = 3 \times 10^{-15}\ cm^3\ s^{-1/2}$ is the rate constant for singlet−singlet annihilation process, and $k_{bp} = 7.1 \times 10^9\ s^{-1}$ is the rate constant for the back photoisomerization.

excited state of the monomers to the signals has been removed by means of the SVD analysis according to the previous discussion. Thus, decays shown in Figure 5 only represent deactivation of the excited aggregates. In addition to that, no changes in the shape of the transient absorption bands after the SVD analysis (Figure S9) were observed under different laser excitation fluences. The *y*-axis of the Figure 5 represents the density of singlet excited states of the aggregates in the film per cm^3. We have calculated its value assuming that, at zero time, $n(t) = n(0)$, where $n(0)$ is the density of singlet excited states formed by the pump, and that one absorbed photon produces one first singlet state. Additionally, we have estimated a pump

dx.doi.org/10.1021/jp210281z | J. Phys. Chem. C 2012, 116, 9379−9389

spot diameter of 0.15 mm, and the measured sample thickness is ≈ 60−70 nm (using a surface profiler). We noted that the initial photoinduced signal scales linearly with the pump fluence even at excited states densities having strong interaction. This precludes the existence of higher order nonlinear effects (e.g., further excitation to a higher excited state or excitation of a biexciton). On the other hand, we noticed that an increase in the pump fluence produces a much faster deactivation of the excited state. This phenomenon indicates singlet−singlet annihilation process, for which a high density of excited states brings the species into close proximity, favoring this mechanism. In fact, a multiexponential fit of the signal reveals that the amplitude for the faster component gets larger when the fluence increases. However, an accurate analysis of the data according to a singlet−singlet exciton annihilation process requires a more complex kinetics scheme. Thus, the dynamics of the first singlet excited states of the aggregates can be modeled by the following differential rate equation:[35]

$$\frac{dn}{dt} = -kn - \gamma n^2 \tag{2}$$

where n is the density of the singlet excited states of the aggregates, k is the rate constant in the absence of any interaction between excitons, and γ is the exciton rate constant via bimolecular annihilation process. The latter can be either time-independent, reflecting the hopping migration of excitons in the crystallites, or time-dependent, in particular $\gamma = \gamma' t^{-1/2}$ (γ' is the time-independent decay rate constant) accounting for an annihilation process via a three-dimensional Förster-type dipole−dipole interaction between excitons or via one-dimensional exciton diffusion.[35] In the time-independent case, eq 2 can be easily integrated to lead to a fitting equation. Attempts to fit the experimental data at any laser fluence were unsuccessful. This suggests that the annihilation rate constant (γ) contains substantial time dependence, and then the integration of eq 2 becomes more complex. By taking into account the model for which $\gamma = \gamma' t^{-1/2}$, we can solve eq 2 and express the integrated rate law as follows:

$$\frac{n}{n_0} = \frac{\exp(-kt)}{1 + \left(\frac{2n_0\gamma'}{\sqrt{k}}\right)\mathrm{erf}(\sqrt{kt})} \tag{3}$$

$$\mathrm{erf}(x) = \frac{2}{\sqrt{\pi}}\int_0^{\infty} \exp(-x^2)\,dx \tag{4}$$

where erf(x) is the Gauss error function and $x = (kt)^{1/2}$. The fitted curves based on eqs 3 and 4 for SQ 26 and SQ 41 are shown in Figure 5, and the calculated rate constants are listed in Table 2. These data give information on the aggregates deactivation process. An aspect to support the consistency of the model is that the rate constants values are quite similar to each other regardless of the pump fluence. For example, the γ' value for SQ 26 only varies 15% (3.3 to 2.8 × 10^{-15} cm^3 s$^{-1/2}$) when the energy fluence changes from 100 to 500 nJ/pulse, and it is almost the same for 100 and 250 nJ/pulse (3.3 to 3.1 × 10^{-15} cm^3 s$^{-1/2}$). Notice that the rate constant values of k in the absence of any interaction between excitons are not very different from those of the monomers in solution ($k \sim 2 \times 10^{10}$ s^{-1}). Regarding γ', we estimated an average value of 3.1 × 10^{-15} and 3.3 × 10^{-15} cm^3 s$^{-1/2}$ for SQ 26 and SQ 41, respectively. We noticed small differences between the γ' values of SQ 26 and SQ 41. This suggests that the COOH groups (one in SQ 41 and two in SQ 26) do not play a major role in the packing and aggregation in the solid state, and therefore they are mainly governed by $\pi-\pi$ interactions. The knowledge of these rate constants might be useful in the analysis of the transient signals of other samples containing H- or J-aggregates of comparable SQs. Dye-sensitized solar cells (DSSCs) prepared with SQs may have a strong aggregation, giving rise to H- or J-aggregates.[32c] Thus, knowing the γ' values of SQs, it is possible to calculate the rate constant for electron injection into the used material (TiO_2, for example) and which is a very important parameter in the operation of DSSCs.

Table 2. Values of the Decay Rate Constants, k, in the Absence of Exciton Interaction, and Annihilation Rate Constant, γ' from the Singlet−Singlet Annihilation Model for SQ 26 and SQ 41 Aggregates at the Three Fluences of the Pump[a]

sample	E_{exc} (nJ pulse^{-1})	$k \times 10^{-10}$ (s^{-1})	$\gamma' \times 10^{15}$ (cm^3 s$^{-1/2}$)	$k_{bp} \times 10^{-7}$ (s^{-1})
SQ 26	100	2.4	3.3	3.3
	250	1.6	3.1	
	500	1.5	2.5	
SQ 41	100	0.5	4.5	2.8
	250	1.6	2.7	
	500	5.0	2.8	

[a] k_{bp} is the rate constant for the back photoreaction of the *cis* photoisomers of the aggregates in thin films.

We now turn our attention to describe the possible physical mechanisms that govern the annihilation process. The rate-limiting step of this bimolecular reaction may involve two main mechanisms: either energy transfer itself as it would occur from a long-range Förster-type mechanism or diffusion of the excitons between the neighboring SQ molecules to give an interaction by collisional- or Dexter-type process.[39] Exciton diffusion mechanism follows the next equation for the annihilation rate constant, assuming that the excitons are particles with an isotropic diffusion constant D, which annihilates if a pair of particles comes closer than a critical distance, R:[39,40]

$$\gamma = 4\pi DR\left(1 + \frac{R}{\sqrt{\pi Dt}}\right) \tag{5}$$

It is important to remark that the annihilation process for the SQs occurs in the picosecond time scale (see the time profiles of Figure 5); therefore, this time window is used in the following discussion. We distinguish two regimes: (a) a high-diffusion limit where $D > R^2/(\pi t)$ and then $\gamma \approx 4\pi DR$; (b) a low-diffusion limit where $D < R^2/(\pi t)$ and then $\gamma \approx \gamma' t^{-1/2}$. In the high-diffusion limit, the annihilation rate constant no longer contains any intrinsic time dependence. This result is in opposition with the experimental time dependence. Therefore, we rule out a fast diffusion process (high values of D) to account for the interaction of the excitons. The low-diffusion limit leads to the same time dependence, $\gamma = \gamma' t^{-1/2}$, used to accurately fit the experimental data, with a time-independent constant $\gamma' = 4R^2(\pi D)^{1/2}$. In this limit, however, D would be still very small ($D \approx 2 \times 10^{-3}$ cm^2 s^{-1}). The distance traveled by an exciton in 1 ps ($r = (Dt)^{1/2} \sim 0.5$ nm) would be too short to account for the strong quenching of the transient signal at early times. Thus, we conclude that diffusion of excitons in this case is not the limiting step of the bimolecular annihilation dynamics, although it can be an important factor at longer times (after 100 ps).

dx.doi.org/10.1021/jp210281z | J. Phys. Chem. C 2012, 116, 9379−9389

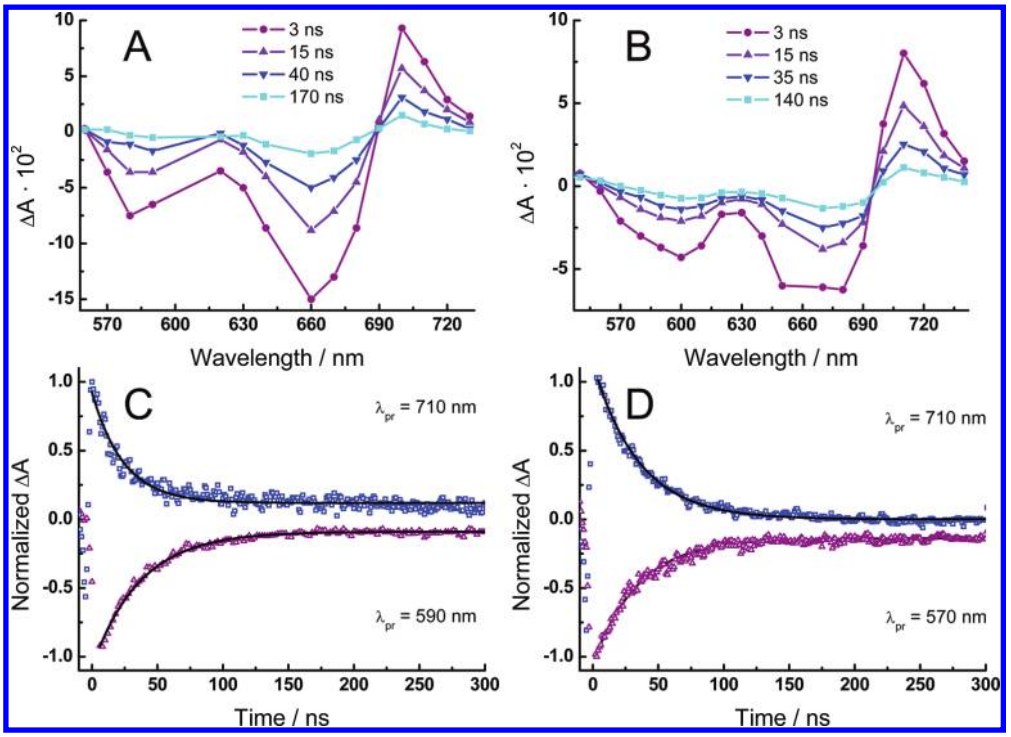

Figure 6. Upper: nanosecond transient absorption spectra reflected in the change of absorbance (ΔA) of SQ 41 (A) and SQ 26 (B) deposited as thin films on quartz plates at 3, 15, 40, and 170 ns after the laser pulse. Lower: normalized time profiles of SQ 41 (C) and SQ 26 (D). The probed wavelengths are indicated in the inset. The solid lines represent the best fit using a single-exponential function.

In the second mechanism, long-range dipole−dipole interaction, Förster theory[41] predicts a $t^{-1/2}$ dependence of the annihilation rate constant, which matches with the experimental observation. Thus, time-independent rate constant, γ', is given by

$$\gamma' = \frac{2\pi R_0^3}{3}\sqrt{\frac{\pi}{\tau}} \tag{6}$$

where R_0 is the distance between the dipoles at which the decay rate due to dipole−dipole interaction is equal to the natural decay given by $1/\tau$. At distances longer than R_0, the bimolecular decay via Förster process is ineffective. We obtained a value of $R_0 \approx 2.5$ nm. This distance is considerably longer than the one deduced using the low-diffusion limit. However, it is in agreement with the interaction between excitons at low pump fluence, at which they are away from each other. SQs present a small Stokes shift, which makes the spectral overlap integral between donor and acceptor spectra very large. Moreover, the absorption coefficient is also very high. These features suggest that long-range Förster-type energy transfer process should be very efficient in these SQs. We calculated the Förster-radius in an ACN solution by using the equation

$$R_0^6 = \frac{9000(\ln 10)\kappa^2\Phi_{SQ}}{128\pi^5 N n^4}\int F_{SQ}(\lambda)\varepsilon_{SQ}(\lambda)\lambda^4\, d\lambda \tag{7}$$

where κ^2 is the factor describing the relative orientation of the dipoles in the ground and excited state, assumed to be equal to 2/3, Φ_{SQ} is the fluorescence quantum yield in the absence of energy transfer for a given SQ, F_{SQ} is the normalized fluorescence, ε_{SQ} is the absorption coefficient at the absorption wavelength (λ), n is the refractive index of the medium, and N is Avogdro's number. A Förster radius of 5.7 nm is estimated for these SQ molecules in acetonitrile solutions, which is longer than that calculated by the annihilation rate constant (2.5 nm). However, we have to consider the formation of H- and J-aggregates in the solid state with respect to the samples in solution, which reduces considerably the emission of the SQs and enlarges the absorption band of the SQs to the blue side, decreasing the overlap with the emission band.

Finally, we compared the R_0 estimated from the annihilation rate constant with the average distance of the excitons at the lowest fluence of the pump (100 nJ/pulse) used in our experiments. An estimate of the molecular density gives $N_0 = 6 \times 10^{20}$ molecules cm^{-3}.[42] The average distance can be calculated by using $\Delta x = aN_0/n_0$, where a is the lattice constant, $a \approx 0.7$ nm, and n_0 is the initial density of the singlet excited states.[43] We got 7 nm as an average distance between excitons at low energies, which is much longer than the 2.5 nm at which the long-range Förster-type process is not operative. Thus, there must be an additional factor that increases the distance at which the excitons can interact to each other. This additional process must be the spatial extent of the exciton itself, that is, the quantum delocalization of the wave function of the exciton in the aggregates. Quantum delocalization over distances greater that 5 nm has been reported to occur in similar compounds,[44] which supports the feasibility of the annihilation process in these SQs at long distances.

To summarize this section, SVD analysis of the fs transient signal proves the presence of two excited species, monomer and aggregates, and permits to separate the dynamics of each one. For SQ monomers, the singlet excited state behavior does not depend on the pump fluence, and we thus propose that the quenching of the excited monomers is due to an energy transfer to the aggregates (in the ground state). On the other hand, transient signals of the aggregates are strongly dependent on the pump fluence, and we thus found that a singlet−singlet exciton annihilation process is responsible of the fast

dx.doi.org/10.1021/jp210281z | J. Phys. Chem. C 2012, 116, 9379−9389

deactivation of the excited aggregates. Long-range Förster-type interactions between excitons together with the intrinsic delocalization of the excitons in the aggregates appear as the physical mechanism involved in the annihilation of the excitons.

3.4. Nanosecond Flash Photolysis Measurements. The fs−ps transient absorption signals (Figure S4) showed a weak positive peak at 710 nm, which is due to a long-living species (>1 ns). Thus, we performed ns−μs transient absorption experiments using the flash photolysis setup to investigate the nature of this component.

Figure 6 exhibits the results for SQ 41 and SQ 26 films at four delay times. The excitation wavelength was 650 and 660 nm for SQ 41 and SQ 26, respectively. We found positive features at 700−730 nm and two bleaching bands at 580−600 and 650−680 nm, with a "valley" around 625 nm between the two negative signals. The negative signals are assigned to the ground state bleach, since they are coincident with the steady-state absorption spectra. However, there is one important difference: the absence of signal at 625 nm, corresponding to the monomer absorption maximum. Consequently, the involvement of excited SQ monomers signal on this time scale is ruled out. Moreover, triplet state of SQs has been reported not to be formed by straightaway intersystem crossing from the singlet since its quantum yield is rather insignificant ($\Phi_{ISC} < 0.001$).[45,46] Finally, the ns-transient absorption features resemble those observed in solution,[34,37] with a 50 nm red-shift for the solid film spectra (Figure S12). It is worth remembering that the transient signals in solution were ascribed to the *cis* photoisomer of the SQs that is formed after a very fast twisted intramolecular charge-transfer process.[34,47] The decay of the transient signals in solution in the μs time scale was attributed to a *cis*−*trans* back-photoisomerization, recovering the initial ground state of the SQs.[34,48] From the above-mentioned discussion and experimental observation, we conclude that the transient signal at 710 nm in the solid state must be attributed to the *cis* photoisomers of the J-aggregates (Scheme 1). We also expect the formation and decay of the *cis* photoisomers of the H-aggregates, whose transient signal should appear around 650 nm. However, we did not observe this transient signal most probably because it is overlapped with the intense bleaching band.

The fits of the time profiles of the absorption changes at the two negative signals produced identical lifetimes (30 and 35 ns for SQ 41 and SQ 26, respectively). Therefore, they originate from the same state. If we extend the fits to the other probing wavelengths (positive signal), we obtain the same values (Figure 6). The presence of both H- and J-aggregates in the photodynamics of solid sample of SQs, and the observation of a single lifetime in the whole spectral range suggest that the back-photoisomerization reaction has similar rate constant (k_{bp}) for the *cis* photoisomers of both H- and J-aggregates (Scheme 1). To further investigate if the deactivation process is affected by the type of the excited aggregates, we have pumped the films at different excitation wavelengths, 590, 640, and 670 nm, which mainly correspond to the H-aggregates, monomers, and J-aggregates absorption, respectively (Figure S13). We recorded the same transient absorption spectra with similar time constants. This result indicates that the deactivation of the excited state of the H- and J-aggregates produce similar twisted states that eventually transform into the *cis* photoisomers.

Photoisomerization of *trans* isomers to the *cis* one in the solid state of organic compounds is a well-known reaction that possesses high selectivity.[49] Although the final products might not be different from those formed by a photoisomerization in solution, the mechanism of crystal-to-crystal reactions proceeds in a different way. Comparison of the slow transient dynamics in solid state with that in solution reveals shorter lifetimes in the solid sample, 14 ns vs 1.6 μs in ACN for SQ 26. The twisting process has to compete with the rapid annihilation process; otherwise, the *cis* photoisomer would not have been detected. In conclusion, *trans*−*cis* photoisomerization also takes place in thin films but, in this case, in the aggregates. As a possible explanation, $\pi-\pi$ interactions within the aggregates should be coupled to the intramolecular charge transfer (ICT) within the involved monomers moieties. The twisting at the excited state of the SQs should be strongly coupled to the ICT process. Thus, $\pi-\pi$ interactions should play a role in the isomerization process at both ground and excited state. This might be the reason why the back-isomerization (*cis* to *trans*) is faster in solid than in solution, where we only observed the dynamics of monomers.

4. CONCLUSION

Solid-state thin films of the studied SQs show the presence of H- and J-aggregates. This is reflected by the broadening and red-shift of the absorption bands together with the enhanced scattering signals at the absorption wavelengths. The formation of H- and J-aggregates in these SQs depends on the type of alkyl chain at the N-position in the indole moiety. On the other hand, fs−ps transient UV−vis absorption experiments showed a faster relaxation of the excited state in relation to that in solution, and which involves different deactivation pathways. The associated transient spectra for the fastest component (<1 ps) are similar to those in solution, ascribing its dynamics to the deactivation of the first singlet excited state of the monomer species. On the other hand, the associated spectra for the long-living component (>1 ps) are attributed to the excited state of the H- and J-aggregates. Singular value decomposition (SVD) analysis of the data together with the dependence of the transient signals on the pump fluence permitted to identify the relaxation mechanisms involved in the thin films.

Scheme 1 summarizes the two quenching processes that affect the electronically first excited states of the involved species. On one hand, the S_1 state of the monomer undergoes an energy transfer process to the aggregates, exhibiting an extremely fast rate constant for this process, $\approx 10^{13}$ s^{-1}. On the other hand, singlet−singlet annihilation mechanism accounts for the deactivation of the aggregates, $\gamma' \approx 3 \times 10^{-15}$ cm^3 s$^{-1/2}$, since their S_1 state signal shows a strong dependence on the pump fluence. Long-range Förster-type interactions between excitons together with their intrinsic delocalization in the aggregates appear as the mechanism involved in their annihilation.

Regarding the ns-flash photolysis experiments, positive and negative transient signals, and decay time constant of about 30−35 ns are attributed to the *cis* photoisomer of the aggregates. The lifetimes of the *cis* photoisomers in the films are 2 orders of magnitude shorter than in solution. The behavior is explained in terms of a different mechanism of the crystal-to-crystal back-photoisomerization, where $\pi-\pi$ interactions within the aggregate should play a role in the photocycle. The importance of this work resides in the relevance of the involved mechanism of monomers and aggregates photodynamics in the working scheme of SQs in the solid state for many photonic applications, for example, in dye-sensitized solar cells (DSSCs and LEDs) Thus, this work

dx.doi.org/10.1021/jp210281z | J. Phys. Chem. C 2012, 116, 9379−9389

will be valuable for a better understanding the operation of SQ molecular systems and in designing new electronic devices with improved properties, where such kinds of dyes are used.

■ ASSOCIATED CONTENT

Supporting Information

Figures S1−S13. This material is available free of charge via the Internet at http://pubs.acs.org.

■ AUTHOR INFORMATION

Corresponding Author

*E-mail: Abderrazzak.douhal@uclm.es.

Present Address

[§]Center for Ultrafast Laser Spectroscopy, A. Mickiewicz University, Umultowska 85, 61-614 Poznan, Poland.

Notes

The authors declare no competing financial interest.

■ ACKNOWLEDGMENTS

This work was supported by the MICINN through projects PLE2009-0015 and MAT2008-01609. M.Z. thanks the support from the European Community's Seventh Framework Programme (FP7/2007-2013) under grant agreement no. 235286 (NANOSOL), and G.M. is grateful to MICINN for a "Juan de la Cierva" contract.

■ REFERENCES

(1) Kobayashi, T. *J-aggregate*; World Scientific: Singapore, 1996.

(2) (a) Deisenhofer, J., Norris, J. R., Eds.; *The Photosynthetic Reaction Center*; Academic Press: San Diego, 1993. (b) Blankenship, R. E., Madigan, M. T., Bauer, C. E., Eds.; *Anoxygenic Photosynthetic Bacteria*; Kluwer Academic Publishing: Dordrecht, The Netherlands, 1995.

(3) Zietz, B.; Prokhorenko, V. I.; Holzwarth, A. R.; Gillbro, T. *J. Phys. Chem. B* **2006**, *110*, 1388−1393.

(4) Bixon, M.; Jortner, J. *Electron Transfer-From Isolated Molecules to Biomolecules*; Bixon, M., Jortner, J., Eds.; John Wiley & Sons: New York, 1999; Part 1, pp 35−202.

(5) Balzani,V., Ed.; *Electron Transfer in Chemistry*; Wiley-VCH: Weinheim, 2001.

(6) (a) Gunes, S.; Neugebauer, H.; Sariciftci, N. S. *Chem. Rev.* **2007**, *107*, 1324−1338. (b) Thompson, B. C.; Frechet, J. M. J. *Angew. Chem., Int. Ed.* **2008**, *47*, 58. (c) Imahori, H. *J. Mater. Chem.* **2007**, *17*, 31−41. (d) Segura, J. L.; Martín, N.; Guldi, D. M. *Chem. Soc. Rev.* **2005**, *34*, 31−41.

(7) (a) Slinker, J. D.; Rivnay, J.; Moskowitz, J. S.; Parker, J. B.; Bernhard, S.; Abruña, H. D.; Malliaras, G. G. *J. Mater. Chem.* **2007**, *17*, 2976−2988. (b) Bolink, H. J.; Coronado, E.; Costa, R. D.; Ortí, E.; Sessolo, M.; Graber, S.; Doyle, K.; Neuburger, M.; Housecroft, C. E.; Constable, E. C. *Adv. Mater.* **2008**, *20*, 3910−3913.

(8) Yokoyama, T.; Yokoyama, S.; Kamikado, T.; Okuno, Y.; Mashiko, S. *Nature* **2001**, *413*, 619−621.

(9) Micali, N.; Mallamace, F.; Romeo, A.; Purrello, R.; Monsu Scolaro, L. *J. Phys. Chem. B* **2000**, *104*, 5897−5904.

(10) Rubires, R.; Farrera, J. A.; Ribó, J. M. *Chem.—Eur. J.* **2001**, *7*, 436−446.

(11) Maiti, N. C.; Ravikanth, M.; Mazumdar, Sh.; Periasamy, N. *J. Phys. Chem.* **1995**, *99*, 17192−17197.

(12) Spano, F. C. *Acc. Chem. Res.* **2010**, *43*, 429−439.

(13) (a) Fidder, H.; Knoester, J.; Wiersma, D. A. *Chem. Phys. Lett.* **1990**, *171*, 529. (b) Scholes, G. D.; Rumbles, G. *Nat. Mater.* **2006**, *5*, 683−696.

(14) Moll, J.; Dähne, S.; Durrant, J. R.; Wiersma, D. A. *J. Chem. Phys.* **1995**, *102*, 6362−6370.

(15) de Boer, S.; Wiersma, D. A. *Chem. Phys. Lett.* **1990**, *165*, 45−53.

(16) Minoshima, K.; Taiji, M.; Misawa, K.; Kobayashi, T. *Chem. Phys. Lett.* **1994**, *218*, 67−72.

(17) Möbius, D. *Adv. Mater.* **1995**, *7*, 437−444.

(18) (a) Alex, S.; Basheer, M. C.; Arun, K. T.; Ramaiah, D.; Das, S. *J. Phys. Chem. A* **2007**, *111*, 3226−3230. (b) Mor, G. K.; Kim, S.; Paulose, M.; Varghese, O. K.; Shankar, K.; Basham, J.; Grimes, C. A. *Nano Lett.* **2009**, *12*, 4250−4257.

(19) (a) Ajayaghosh, A. *Acc. Chem. Res.* **2005**, *38*, 449−459. (b) Beverina, L.; Salice., P. *Eur. J. Org. Chem.* **2010**, 1207−1225. (c) Eldo, J.; Ajayaghosh., A. *Chem. Mater.* **2002**, *14*, 410−418.

(20) Law, K. Y. *J. Phys. Chem.* **1987**, *91*, 5184−5193.

(21) Sauve, G.; Kamat, P. V.; Thomas, K. G.; Thomas, K. J.; Das, S.; George, M. V. *J. Phys. Chem.* **1996**, *100*, 2117−2124.

(22) Xu, Y.; Li, Z.; Malkovskiy, A.; Sun, S.; Pang, Y. *J. Phys. Chem. B* **2010**, *114*, 8574−8580.

(23) Gayathri Devi, D.; Cibin, T. R.; Ramaiah, D.; Abraham, A. *J. Photochem. Photobiol., B* **2008**, *92*, 153−159.

(24) Ziegenbein, W.; Sprenger, H.-E. *Angew. Chem., Int. Ed.* **1966**, *5*, 893−894.

(25) Bonnett, R.; Motevalli, M.; Siu, J. *Tetrahedron* **2004**, *60*, 8913−8918.

(26) (a) Pandey, S. S.; Inoue, T.; Fujikawa., N.; Yamaguchi, Y.; Hayase, S. *Thin Solid Films* **2010**, *519*, 1066−1071. (b) Inoue, T.; Pandey, S. S.; Fujikawaa, N.; Yamaguchi, Y.; Hayase, S. *J. Photochem. Photobiol., A* **2010**, *213*, 23−29. (c) Pandey, S. S.; Inoue, T.; Fujikawa, N.; Yamaguchi, Y.; Hayase, S. *J. Photochem. Photobiol., A* **2010**, *214*, 269−275.

(27) Bigelow, R.; Freund, H. *Chem. Phys.* **1986**, *107*, 159−174.

(28) (a) Jyothish, K.; Avirah, R. R.; Ramaiah, D. *Org. Lett.* **2005**, *7*, 111−114. (b) Volkova, K. D.; Kovalska, V. B.; Tatarets, A. L.; Patsenker, L. D.; Kryvorotenko, D. V.; Yarmoluk, S. M. *Dyes Pigm.* **2007**, *72*, 285−292.

(29) Marder, S. R. *J. Mater. Chem.* **2009**, *19*, 7392−7393.

(30) Chen, C.-T.; Marder, S. R.; Cheng, L.-T. *J. Am. Chem. Soc.* **1994**, *116*, 3117−3118.

(31) (a) Kuang, D.; Walter, P.; Nüesch, F.; Kim, S.; Ko, J.; Comte, P.; Zakeeruddin, S M.; Nazeeruddin, M. K.; Grätzel, M. *Langmuir* **2007**, *23*, 10906−10909. (b) Geiger, T.; Kuster, S.; Yum, J.-H.; Moon, S.-J.; Nazeeruddin, M. K.; Grätzel, M.; Nüesch, F. *Adv. Funct. Mater.* **2009**, *19*, 2720−2727.

(32) (a) Choi, H.; Raabe, I.; Kim, D.; Teocoli, F.; Kim, C.; Song, K.; Yum, J.-H.; Ko, J.; Nazeeruddin, M. D.; Grätzel., M. *Chem.—Eur. J.* **2010**, *16*, 1193−1201. (b) Choi, H.; Kim, J.-J.; Song, K.; Ko, J.; Nazeeruddin, M. D.; Grätzel., M. *J. Mater. Chem.* **2010**, *20*, 3280−3286. (c) Unger, E. L.; Morandeira, A.; Persson, M.; Zietz, B.; Ripaud, E.; Leriche, P.; Roncali, J.; Hagfeldt, A.; Boschloo, G. *Phys. Chem. Chem. Phys.* **2011**, *13*, 20172−20177.

(33) Gil, M.; Douhal, A. *Chem. Phys.* **2008**, *350*, 179−185.

(34) de Miguel, G.; Marchena, M. J.; Zitnan, M.; Pandey, S. S.; Hayase, S.; Douhal, A. *Phys. Chem. Chem. Phys.* **2012**, *14*, 1796−1805.

(35) (a) Terasaki, A.; Hosoda, M.; Wada, T.; Tada, H.; Koma, A.; Yamada, A.; Sasabe, H.; Garito, A. F.; Kobayashi, T. *J. Phys. Chem.* **1992**, *96*, 10534−10542. (b) Cook, S.; Liyuan, H.; Furube, A.; Katoh, R. *J. Phys. Chem. C* **2010**, *114*, 10962−10968. (c) Ito, F.; Inoue, T.; Tomita, D.; Nagamura, T. *J. Phys. Chem. B* **2009**, *113*, 5458−5463.

(36) Chen, W. G.; Braiman, M. S. *Photochem. Photobiol.* **1991**, *54*, 905−910.

(37) Yamaguchi, S.; Hamaguchi, H. *Chem. Phys. Lett.* **1998**, *287*, 694−700.

(38) Ernsting, N. P.; Kovalenko, S. A.; Senyushkina, T.; Saam, J.; Farztdinov, V. *J. Phys. Chem. A* **2001**, *105*, 3443−3453.

(39) Dogariu, A.; Vacar, D.; Heeger, A. J. *J. Phys. Rev. B* **1998**, *58*, 10218−10224.

(40) (a) Powell, R. C.; Kepler, R. G.; Powell, R. C.; Soos, Z. G. *J. Lumin.* **1975**, *11*, 1−45. (b) Powell, R. C.; Kepler, R. G., Eds.; *Molecular Crystal and Liquid Crystals*; Gordon and Breach: New York, 1970; Vol. *11*, p 349.

(41) (a) Förster, T. *Ann. Phys. (Leipzig)* **1948**, *2*, 55−75. (b) Förster, T. *Z. Naturforsch., A* **1949**, *4A*, 321−327. (c) Förster, T. *Discuss.*

Faraday Soc **1959**, *27*, 7−17. (d) Förster, T. In *Modern Quantum Chemistry*, Istanbul Lectures; Sinanoglu, O., Ed.; Academic: New York, 1965; Vol. *III*, p 93.
(42) To estimate the molecular density, we rinsed one of the fresh solid samples with a certain volume of ACN and measure the absorption of this solution. We determined the total number of molecules in the solid sample by using the extinction coefficient of the SQs. The volume occupied by the molecules in the solid sample is estimated by measuring the area of the sample and the thickness of the SQ thin film, ∼65 nm, supposing that the film is homogeneous. Finally, the number of SQ molecules is divided by the volume to determine the molecular density.
(43) (a) Wöbkenberg, P. H.; Labram, J. G.; Swiecicki, J.-M.; Parkhomenko, K.; Sredojevic, D.; Gisselbrecht, J.-P.; de Leeuw, D. M.; Bradley, D. D. V.; Djukic, J.-P.; Anthopoulos, T. P. *J. Mater. Chem* **2010**, *20*, 3673−3680. (b) Ashwell, G. J.; Roberts, M. P. S.; Rees, N. D.; Bahra, G. S.; Brown, C. R. *Langmuir* **1998**, *14*, 5279−5284.
(44) Kohler, A.; d. Santos, A.; Beljonne, D.; Shuai, Z.; Bredas, J.-L.; Holmes, A. B.; Kraus, A.; Mullen, K.; Friend, R. H. *Nature (London)* **1998**, *392*, 903−906.
(45) Wojcik, A.; Nicolaescu, R.; Kamat, P. V.; Chandrasekaran, Y.; Patil., S. *J. Phys. Chem. A* **2010**, *114*, 2744−2750.
(46) Degassing of solid samples with N_2 did not modify the lifetimes.
(47) (a) Gude, C.; Rettig, W. *J. Phys. Chem. A* **2000**, *104*, 8050−8057. (b) Cornelissen-Gude, C.; Rettig, W.; Lapouyade, R. *J. Phys. Chem. A* **1997**, *101*, 9673. (c) Grabowski, Z. R.; Rotkiewicz, K.; Rettig, W. *Chem. Rev.* **2003**, *103*, 3899−4032.
(48) Tatikolov, A. S.; Costa, S. M. B. *J. Photochem. Photobiol., A* **2001**, *140*, 147−156.
(49) Matsumoto, A. *Top. Curr. Chem.* **2005**, *254*, 263−302.